Research article Open Access

Ya Han, Yan-Ge Liu*, Zhi Wang, Wei Huang, Lei Chen, Hong-Wei Zhang and Kang Yang

Controllable all-fiber generation/conversion of circularly polarized orbital angular momentum beams using long period fiber gratings

DOI 10.1515/nanoph-2017-0047
Received April 30, 2017; revised June 5, 2017; accepted June 11, 2017

Abstract: Mode-division multiplexing (MDM) is a promising technology for increasing the data-carrying capacity of a single few-mode optical fiber. The flexible mode manipulation would be highly desired in a robust MDM network. Recently, orbital angular momentum (OAM) modes have received wide attention as a new spatial mode basis. In this paper, we firstly proposed a long period fiber grating (LPFG) system to realize mode conversions between the higher order LP core modes in four-mode fiber. Based on the proposed system, we, for the first time, demonstrate the controllable all-fiber generation and conversion of the higher order LP core modes to the first and second order circularly polarized OAM beams with all the combinations of spin and OAM. Therefore, the proposed LPFG system can be potentially used as a controllable higher order OAM beam switch and a physical layer of the translating protocol from the conventional LP modes communication to the OAM modes communication in the future mode carrier telecommunication system and light calculation protocols.

Keywords: fiber gratings; higher order linearly polarized modes; orbital angular momentum beams.

1 Introduction

As one of the most fundamental physical quantities in classical and quantum electrodynamics, orbital angular momentum (OAM) of light has initiated widespread interest in many areas, including optical tweezers [1], atom manipulation [2–4], nanoscale microscopy [5], quantum information processing, and large-capacity optical communication [6–8]. A beam of light carrying OAM possesses a phase $\phi(l,\varphi)=\exp(il\varphi)$ in the transverse plane, where φ is the azimuth angle and l is the topological charge number. As the unique characteristics of the OAM light beam were found, a number of attempts to generate and manipulate the OAM beams were proposed based on discrete free space optical systems [6–11] and optical fiber components [12–18].

Conventionally, in optical fibers, the linearly polarized (LP) mode basis is widely used because the modes forming this basis are more readily excited and detected than the eigenmodes [7, 19–21]. Recently, OAM modes stably propagating in fiber-based transmission links have also shown the potential applications in optical communication. Such modes have unlimited topological charge and will reduce propagating OAM modes coupling [12–19]. These two sets of modes have a common eigenmode set in fibers, and therefore, the transformation of modal state between LP modes and OAM modes becomes possible. For example, Li et al. [16] demonstrated the selective conversion from the LP_{11} core modes to the LP-$OAM_{\pm1}$ mode in two-mode fiber (2MF) by utilizing a mechanical long period gratings and a metal parallel slab. Additionally, the eigenmodes in fibers also can be combined to form OAM modes. Zhao et al. [17] generated the $OAM_{\pm1}$ modes composed of $HE_{21}^{even} \pm iHE_{21}^{odd}$ in 2MF based on a CO_2 laser induced titled-long period fiber grating (LPFG). Zhang et al. [18] generated the $OAM_{\pm2}$ modes composed of $HE_{31}^{even} \pm iHE_{31}^{odd}$ in a four-mode fiber (4MF) by using an acoustically induced fiber grating. However, these published works lack analysis in the photonics spin of the generated OAM beams, which is not only a fundamental physical question but also a crucial factor in multiplexing [7] and micro-particles manipulation system [21–23].

***Corresponding author: Yan-Ge Liu,** Key Laboratory of Optical Information Science and Technology, Ministry of Education, Tianjin Key Laboratory of Optoelectronic Sensor and Sensing Network Technology, Institute of Modern Optics, Nankai University, Tianjin 300350, China, e-mail: ygliu@nankai.edu.cn.
http://orcid.org/0000-0003-3428-5692
Ya Han, Zhi Wang, Lei Chen, Hong-Wei Zhang and Kang Yang: Key Laboratory of Optical Information Science and Technology, Ministry of Education, Tianjin Key Laboratory of Optoelectronic Sensor and Sensing Network Technology, Institute of Modern Optics, Nankai University, Tianjin 300350, China
Wei Huang: College of computer and communication engineering, Tianjin University of Technology, Tianjin 300384, China

In this paper, we proposed an LPFG system in the 4MF for exciting and converting higher order LP modes to circularly polarized OAM (CP-OAM) beams with all the combinations of spin and OAM for the first time. The experimental confirmation of all the spin and OAM combinations compensate the shortage in the previous work. Based on the proposed LPFG system, the LP_{11} core modes were converted to the LP_{21} core modes with a ratio of ~96.8%. Aiding with polarization controllers, LP_{11} core modes and the transformed LP_{21} core modes are converted to all the four sets of first-order circularly polarized OAM ($CP\text{-}OAM_{\pm1}$) beams and the four sets of second-order circularly polarized OAM ($CP\text{-}OAM_{\pm2}$) beams, respectively.

2 Principle and experimental configuration

Conventionally, because of the succinctness in expression and the convenience in application, LP modes are widely used. Therefore, in the current study, it is necessary to find the relation between the LP modes and the CP-OAM modes. Each LP mode group in fibers has four unstable transverse electric field distributions [7, 24]:

$$\begin{pmatrix} \mathrm{LP}_{l,1}^{\mathrm{odd},x} \\ \mathrm{LP}_{l,1}^{\mathrm{even},y} \\ \mathrm{LP}_{l,1}^{\mathrm{even},x} \\ \mathrm{LP}_{l,1}^{\mathrm{odd},y} \end{pmatrix} = F_{l,m} \begin{pmatrix} \sin l\phi & 0 \\ 0 & \cos l\phi \\ \cos l\phi & 0 \\ 0 & \sin l\phi \end{pmatrix} \begin{pmatrix} e_x \\ e_y \end{pmatrix} l \geq 1, \tag{1}$$

where $F_{l,m}$ is the radial field distribution, l is the topological charge number and ϕ is the azimuthal coordinate, e_x and e_y are the Cartesian unit vectors for horizontal and vertical polarization, respectively. These LP modes have been referred to as "pseudo modes" [7, 21], because they are linear combinations of eigenmodes with slightly different effective refractive index (n_{eff}):

$$\begin{pmatrix} \mathrm{LP}_{1,1}^{\mathrm{odd},x} \\ \mathrm{LP}_{1,1}^{\mathrm{even},y} \\ \mathrm{LP}_{1,1}^{\mathrm{even},x} \\ \mathrm{LP}_{1,1}^{\mathrm{odd},y} \end{pmatrix} = \begin{pmatrix} 1 & -1 & 0 & 0 \\ 1 & 1 & 0 & 0 \\ 0 & 0 & 1 & 1 \\ 0 & 0 & -1 & 1 \end{pmatrix} \begin{pmatrix} \mathrm{HE}_{2,1}^{\mathrm{odd}} \\ \mathrm{TE}_{0,1} \\ \mathrm{HE}_{2,1}^{\mathrm{even}} \\ \mathrm{TM}_{0,1} \end{pmatrix} l = 1$$

$$\begin{pmatrix} \mathrm{LP}_{l,1}^{\mathrm{odd},x} \\ \mathrm{LP}_{l,1}^{\mathrm{even},y} \\ \mathrm{LP}_{l,1}^{\mathrm{even},x} \\ \mathrm{LP}_{l,1}^{\mathrm{odd},y} \end{pmatrix} = \begin{pmatrix} 1 & -1 & 0 & 0 \\ 1 & 1 & 0 & 0 \\ 0 & 0 & 1 & 1 \\ 0 & 0 & -1 & 1 \end{pmatrix} \begin{pmatrix} \mathrm{HE}_{l+1,1}^{\mathrm{odd}} \\ \mathrm{EH}_{l-1,1}^{\mathrm{odd}} \\ \mathrm{HE}_{l+1,1}^{\mathrm{even}} \\ \mathrm{EH}_{l-1,1}^{\mathrm{even}} \end{pmatrix} l \geq 2 \tag{2}$$

where the expressions of the eigenmodes in a weakly guiding fiber are [7, 24, 25] as follows:

$$\begin{pmatrix} \mathrm{HE}_{2,1}^{\mathrm{odd}} \\ \mathrm{TE}_{0,1} \\ \mathrm{HE}_{2,1}^{\mathrm{even}} \\ \mathrm{TM}_{0,1} \end{pmatrix} = F_{l,m} \begin{pmatrix} \sin\phi & \cos\phi \\ -\sin\phi & \cos\phi \\ \cos\phi & -\sin\phi \\ \cos\phi & \sin\phi \end{pmatrix} \begin{pmatrix} e_x \\ e_y \end{pmatrix} l = 1$$

$$\begin{pmatrix} \mathrm{HE}_{l+1,1}^{\mathrm{odd}} \\ \mathrm{EH}_{l-1,1}^{\mathrm{odd}} \\ \mathrm{HE}_{l+1,1}^{\mathrm{even}} \\ \mathrm{EH}_{l-1,1}^{\mathrm{even}} \end{pmatrix} = F_{l,m} \begin{pmatrix} \sin l\phi & \cos l\phi \\ -\sin l\phi & \cos l\phi \\ \cos l\phi & -\sin l\phi \\ \cos l\phi & \sin l\phi \end{pmatrix} \begin{pmatrix} e_x \\ e_y \end{pmatrix} l \geq 2 \tag{3}$$

In contrast to LP modes, CP-OAM modes are obtained by the linear combination of degenerated eigenmodes with $\pm\pi/2$ phase shift:

$$\begin{pmatrix} \sigma^{+}\mathrm{OAM}_{+l} \\ \sigma^{-}\mathrm{OAM}_{-l} \\ \sigma^{-}\mathrm{OAM}_{+l} \\ \sigma^{+}\mathrm{OAM}_{-l} \end{pmatrix} = F_{l,m} \begin{pmatrix} 1 & i & 0 & 0 \\ 1 & -i & 0 & 0 \\ 0 & 0 & 1 & i \\ 0 & 0 & 1 & -i \end{pmatrix} \begin{pmatrix} \mathrm{HE}_{l+1,1}^{\mathrm{even}} \\ \mathrm{HE}_{l+1,1}^{\mathrm{odd}} \\ \mathrm{EH}_{l-1,1}^{\mathrm{even}} \\ \mathrm{EH}_{l-1,1}^{\mathrm{odd}} \end{pmatrix}, \tag{4}$$

where σ^{+} and σ^{-} denote left and right circular polarization, respectively. Therefore, the transformation of modal state between LP modes and CP-OAM modes is possible in fibers by tuning transmission matrix weight coefficient in eigenmodes.

The CP-OAM modes were generated in 4MF. The 4MF has a core diameter of 19 μm, a cladding diameter of 125 μm, a core cladding index difference of 0.005, and a uniform pure silica cladding (Yangtze Optical Fiber and Cable Corporation). It supports four groups of core modes from 1500 to 1600 nm, i.e., LP_{01}, LP_{11}, LP_{21}, and LP_{02} modes in the LP modes basis {HE_{11}^{x}, HE_{11}^{y}}, {TE_{01}, $HE_{21}^{\mathrm{even/odd}}$, TM_{01}}, {$HE_{31}^{\mathrm{even/odd}}$, $EH_{11}^{\mathrm{even/odd}}$}, and {$HE_{12}^{x}$, HE_{12}^{y}} modes in the eigenmodes solutions, respectively. In this paper, the LP_{11} and LP_{21} core modes in the 4MF are used to generate the $CP\text{-}OAM_{\pm1}$ and $CP\text{-}OAM_{\pm2}$ beams, respectively. Figure 1 depicts the calculated property of $CP\text{-}OAM_{\pm1}$ and $CP\text{-}OAM_{\pm2}$ beams in the 4MF based on the full vector finite element method (FV-FEM). The $\sigma^{\pm}\mathrm{OAM}_{\pm l}$ beams with aligned spin and OAM consist of the $HE_{l+1,1}^{\mathrm{even/odd}}$ modes (Figure 1A and C). The $\sigma^{\mp}\mathrm{OAM}_{\pm l}$ beams with anti-aligned spin and OAM are composed of the $EH_{l-1,1}^{\mathrm{even/odd}}$ modes (Figure 1D). Although the TE_{01} and

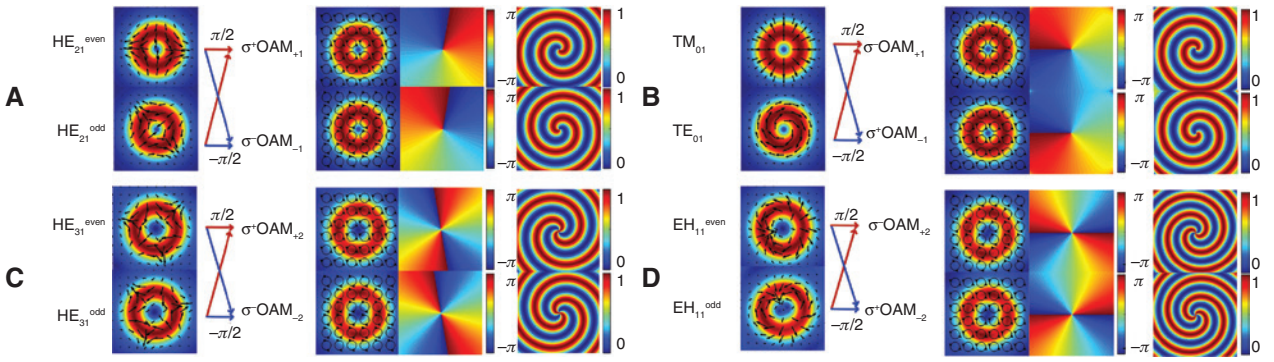

Figure 1: Intensity, polarization, phase, and interferogram of the $\sigma^{\pm}OAM_{\pm1}$ (A), $\sigma^{\mp}OAM_{\pm1}$ (B), $\sigma^{\pm}OAM_{\pm2}$ (C), and $\sigma^{\mp}OAM_{\pm2}$ beams (D).

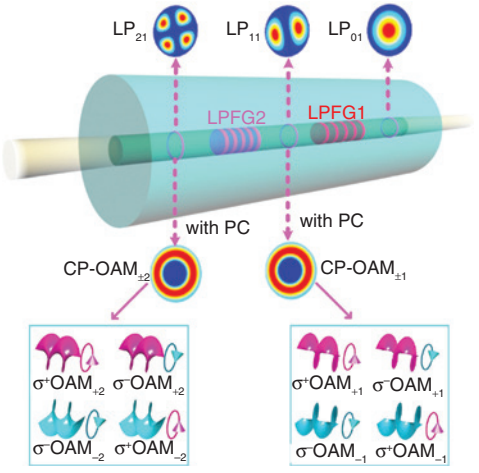

Figure 2: Concept of all-fiber CP-OAM beams generation/conversion.

TM_{01} are not degenerated modes, the linear combination of the TE_{01} and TM_{01} modes with a phase shift of $\pm\pi/2$ also generates $\sigma^{\mp}OAM_{\pm1}$ beams periodically (Figure 1B).

Figure 2 illustrates the principle of all-fiber CP-OAM beams generation/conversion. LPFG1 is designed to transfer LP_{01} core modes to LP_{11} core modes. Adjusting PCs at both ends of LPFG1 converts the LP_{11} modes to all the four sets of CP-$OAM_{\pm1}$ beams ($\sigma^{+}OAM_{+1}$, $\sigma^{-}OAM_{-1}$, $\sigma^{-}OAM_{+1}$, $\sigma^{+}OAM_{-1}$). LPFG2 is connected after LPFG1 to transfer LP_{11} core modes to LP_{21} core modes. Similarly, another PC at the back end of LPFG2 is required to excite the $\sigma^{+}OAM_{+2}$, $\sigma^{-}OAM_{-2}$, $\sigma^{-}OAM_{+2}$, $\sigma^{+}OAM_{-2}$ beams.

The experimental setup of all-fiber CP-$OAM_{\pm1}$ and CP-$OAM_{\pm2}$ beams generation/conversion system is shown in Figure 3. The output beam from a tunable laser (KEYSIGHT, 8164B, N7786B) is divided into two branches by an optical coupler with a proportion of 9:1. The upper branch is used to generate OAM beams, and the lower branch is used as a reference beam to interfere with the generated OAM beams. Two adjustable attenuators ensure same level power distribution in each branch. In the upper branch, PC1 was used to excite different vector modes in the LPFG1. The mode stripper (MS) was used to purify the input beam in 4MF as LP_{01} mode. And then the LP_{01} modes

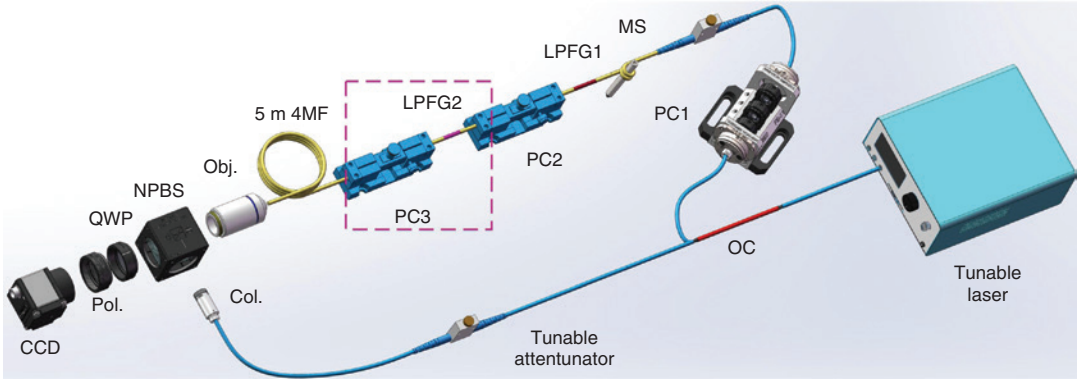

Figure 3: Experiment setup for the generation, conversion, and detection of CP-OAM beams using a circularly polarized interference apparatus.
Col., collimator; LPFG, long-period fiber grating; MS, mode stripper; NPBS, non-polarization beam splitter; QWP, quarter-wave plate; OC, optical coupler; PC, polarization controller; Pol., polarizer.

were converted by LPFG1 to obtain the LP_{11} core modes. To obtain the desired CP-$OAM_{\pm1}$ beams, PC2 was added after the LPFG1 to select vector modes and tune the phase shift between them. In order to generate the CP-$OAM_{\pm2}$ beams, LPFG2 and PC3 in the pink dotted rectangle were aligned after PC2 to convert the LP_{11} core modes to the LP_{21} core modes. To verify the spin and OAM value of the generated beams, a circularly polarized interference apparatus was added after the 4MF output. A 40× objective lens collimated the generated beam. A non-polarization beam splitter (NPBS) combined the two branches to perform spiral interference. A quarter wavelength plate (QWP) was added after NPBS to transfer the CP beams to LP beams. The optical axis of the QWP was fixed at 90°. A rotatable polarizer was aligned after QWP to verify the spin value. Finally, a CCD camera (400–1800 nm, FIND-R-SCOPE-VIS, 85700) recorded the beam patterns.

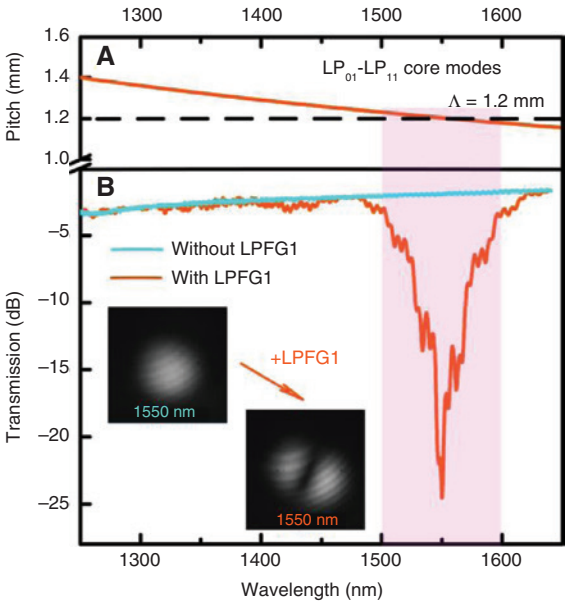

Figure 4: Calculated grating pitches against the resonant wavelength for the mode coupling from LP_{01} core mode to LP_{11} core modes (A); measured transmission spectra of LPFG1 with a period of 1.2 mm and a grating number of 30, and mode profile of the output 4MF at 1550 nm with and without LPFG1, respectively (B).

3 Experimental results and discussions

3.1 Generation of the CP-$OAM_{\pm1}$ beams

To generate the CP-$OAM_{\pm1}$ beams, the LPFG1 was prepared firstly to realize core modes coupling from LP_{01} to LP_{11}. We first calculated the grating period of LPFG1 before fabrication. The phase matching condition in LPFG is [26] as follows:

$$\Lambda = \frac{\lambda}{n_1 - n_2}, \tag{5}$$

where Λ is the grating pitch, λ is the resonant wavelength, and n_1 and n_2 are n_{eff} of the two coupling modes. According to the parameters of 4MF described in Section 2, a 4MF model was built to calculate the n_{eff} of LP_{01}, LP_{11}, and LP_{21} core modes using the FV-FEM. The Sellmeier equation for silica cladding is adopted in the numerical calculation to improve accuracy [27]. Based on the phase-matching condition of LPFGs and the calculated n_{eff} values, the relationship between the calculated grating pitches and resonant wavelength for mode-coupling between the LP_{01} core modes and the LP_{11} core modes in the 4MF is depicted in Figure 4A.

In order to obtain mode coupling around 1550 nm, the pitch and grating number of the LPFG1 are selected as 1.2 mm and 30, respectively, according to Figure 4A. We fabricated the LPFGs by lateral exposing the 4MF with a CO_2 laser (CO_2-H30, Han's laser). A section of 4MF ~50-cm long was core-align spliced with a segment of SMF at both ends with an insertion loss of ~3 dB. The 4MF was axially tensioned with a ~20-g weight. A beam of light from a SLED source (1250–1650 nm, TOP Photonics) was launched into the SMF. The output spectra were measured with an optical spectrum analyzer (OSA, 1200–2400 nm, YOKOGAWA, AQ6375) with a resolution of 0.5 nm. From the measured transmission spectra and mode profiles in Figure 4B, it demonstrates that the LPFG1 is well performed with a low insertion loss of ~0.035 dB and a high conversion ratio of ~96% at 1550 nm. The clear two-lobe mode profile at 1550 nm shows that the LPFG1 converts the LP_{01} core modes to the LP_{11} core mode efficiently. Because of the mode mismatch between the 4MF and SMF, a small amount of higher order core modes was excited at the input interface between the SMF and 4MF, and therefore, mode interference fringes appear around the resonant wavelength of the LPFG1 [28].

After that, the fabricated LPFG1 was put into the apparatus in Figure 3 to generate the CP-$OAM_{\pm1}$ beams (without the components in the pink dotted rectangle). Firstly, the polarization state in the reference beam was set as left circular polarization by adjusting the PC circuit in tunable laser. The σ^+OAM_{+1} and σ^+OAM_{-1} beams were excited selectively by tuning the rotation angle and applied pressure in PC2. In Figure 5A, the helicity of the interference pattern is left-handed spiral, which represents that the topological

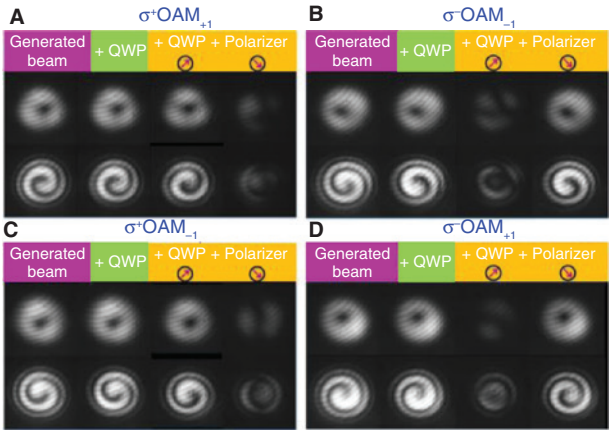

Figure 5: Intensity and interferogram of the generated (A) $\sigma^{+}OAM_{+1}$, (B) $\sigma^{-}OAM_{-1}$, (C) $\sigma^{+}OAM_{-1}$, (D) $\sigma^{-}OAM_{+1}$.

charge number of the OAM is +1. After passing through the QWP and polarizer, the beam profile will be the darkest and brightest when the optical axis of the polarizer is −45° and 45°, respectively. It represents that the spin of the generated beam is left-handed. And thus, the generated beam in Figure 5A is the $\sigma^{+}OAM_{+1}$ beam. In Figure 5C, the helicity of the interference pattern is opposite to that in Figure 5A, but the bright/dark beam situation maintains the same with Figure 5A. This demonstrates that the $\sigma^{+}OAM_{-1}$ beam is generated with an anti-aligned OAM-spin configuration. Then the polarization state in the reference beam was set as right-handed polarization. Similarly, the $\sigma^{-}OAM_{-1}$ (Figure 5B) and $\sigma^{-}OAM_{+1}$ (Figure 5D) beams were selectively excited by tuning PC2 accurately. Additionally, in Figures 5C and 5D, we presented the $\sigma^{\mp}OAM_{\pm1}$ beams, which can only periodically be present in fibers because the TE_{01} and TM_{01} modes possess a different n_{eff}.

3.2 LP_{11} core modes to LP_{21} core modes conversion and generation of the CP-$OAM_{\pm2}$ beams

Flexible mode control in fibers, such as higher order mode conversion, would be highly desired in a robust MDM network. In this section, we proposed an efficient method to detect and convert the higher order LP core modes for the first time. The conversion among the higher order modes in fibers is rarely reported because it suffers from two technical difficulties: the first is how to estimate whether the conversion between higher order modes is sufficient. In the conventional SMF-4MF-SMF aligned LPFG measurement system, the transmission spectra of LPFGs are all dips for any higher order mode. Thus, it is really difficult to distinguish whether the target higher order mode is converted. The second difficulty is how much energy of the target higher order mode is converted.

To tackle these two difficulties, we propose a new fiber alignment of SMF-4MF-2MF. The input of the 2MF was core-aligned to the 4MF with the LPFG1 in Section 3.1, and the output of the 2MF was connected to the OSA. The length of the 2MF was ~30 m. The 2MF is designed by the OFS Company to only support the LP_{01} and LP_{11} core modes at the 1550-nm region. Thus, the resonant dip of LPFG1 disappears when the 2MF was connected to the OSA as a transmission fiber (the blue curve in Figure 6B). Figure 6A depicted the relationship between the calculated grating pitches and resonant wavelength for mode-coupling between the LP_{11} core mode and the LP_{21} core modes in the 4MF. According to Figure 6A, we fabricated the LPFG2 with a period and grating number of 0.954 mm and 40, respectively, to ensure mode coupling around 1550 nm. Because the 2MF cannot transmit LP_{21} mode with low loss, there is a dip at the resonant wavelength (1550 nm), which indicates mode conversion from the LP_{11} core modes to the LP_{21} core modes. Figure 6B demonstrates that the LPFG2 is also well performed with a low insertion loss of ~0.008 dB and high conversion ratio of ~96.8 % at 1550 nm. From the two insets in Figure 6B, the four-lobe mode profile at 1550 nm

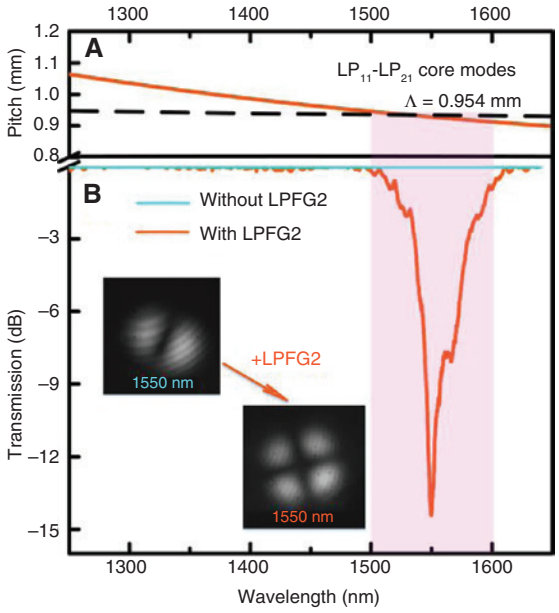

Figure 6: Calculated grating pitches against the resonant wavelength for the mode coupling from LP_{11} core mode to LP_{21} core modes (A); measured transmission spectra of LPFG2 with a period of 0.954 mm and a grating number of 40, and mode profile of the output 4MF at 1550 nm with and without LPFG2, respectively (B).

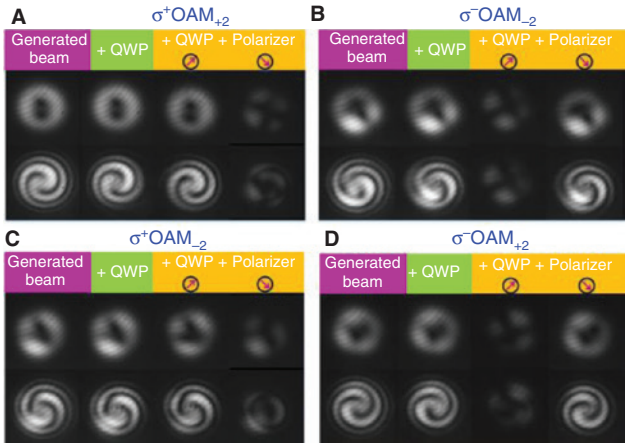

Figure 7: Intensity and interferogram of the generated (A) $\sigma^{+}OAM_{+2}$, (B) $\sigma^{-}OAM_{-2}$, (C) $\sigma^{+}OAM_{-2}$, (D) $\sigma^{-}OAM_{+2}$.

can be found, which represents that LPFG2 converts the LP_{11} core modes to the LP_{21} core mode efficiently.

And then LPFG2 was measured by using the setup in Figure 3 to generate the CP-$OAM_{\pm 2}$ beams (with the pink dotted rectangle). Based on the aforementioned methods in Section 3.1, the $\sigma^{+}OAM_{+2}$ (Figure 7A), $\sigma^{-}OAM_{-2}$ (Figure 7B), $\sigma^{+}OAM_{-2}$ (Figure 7C), and $\sigma^{-}OAM_{+2}$ (Figure 7D) beams are selectively excited by tuning PC2 and PC3 accurately. Although the generated beams with $l=\pm 2$ are not perfect, all the OAM-spin configuration of the CP-$OAM_{\pm 2}$ beams can be verified, which has been predicted in theory over 5 years but never been demonstrated in the experiments.

4 Conclusion

In summary, we firstly proposed a 4MF-LPFG system to realize all-fiber controllable generation and conversion of the CP-$OAM_{\pm 1}$ beams and the CP-$OAM_{\pm 2}$ beams with all the combinations of spin and OAM. Based on the LPFG system, the LP_{11} modes were efficiently converted to the LP_{21} modes with a ratio of ~96.8%. Aiding with polarization controllers, LP_{11} modes and the transformed LP_{21} modes are converted to CP-$OAM_{\pm 1}$ ($\sigma^{+}OAM_{+1}$, $\sigma^{-}OAM_{-1}$, $\sigma^{-}OAM_{+1}$, $\sigma^{+}OAM_{-1}$) and CP-$OAM_{\pm 2}$ ($\sigma^{+}OAM_{+2}$, $\sigma^{-}OAM_{-2}$, $\sigma^{-}OAM_{+2}$, $\sigma^{+}OAM_{-2}$) beams, respectively. The proposed LPFG system would be a potential device to achieve a controllable higher order OAM beam switch, which could enhance the flexibility of data management at network nodes in mode-division multiplexing networks. Additionally, it provides an idea for the translating protocol from the conventional LP modes communication to the OAM modes communication.

Acknowledgments: This work is funded by the National Natural Science Foundation of China (NSFC) (11674177, 61322510, 61640408), Tianjin Natural Science Foundation (16JCZDJC31000, 14JCZDJC31300), and the Natural Science Foundation of Hebei Province (F2014109105). Thank you to Youchao Jiang in Beijing Jiaotong University and Prof. Xiaolei Wang in Nankai University for their kindly discussion.

References

[1] Dholakia K, Čižmár T. Shaping the future of manipulation. Nature Photon 2011;5:335–42.
[2] Paezlopez R, Ruiz U, Arrizon V, Ramosgarcia R. Optical manipulation using optimal annular vortices. Opt Lett 2016;41:4138–41.
[3] Tkachenko G, Brasselet E. Helicity-dependent three-dimensional optical trapping of chiral microparticles. Nat Commun 2014;5:4491.
[4] Padgett M, Bowman R. Tweezers with a twist. Nature Photon 2011;5:343–8.
[5] Fürhapter S, Jesacher A, Bernet S, Ritschmarte M. Spiral interferometry. Opt Lett 2005;30:1953–5.
[6] Wang J, Yang JY, Fazal IM, et al. Terabit free-space data transmission employing orbital angular momentum multiplexing. Nature Photon 2012;6:488–96.
[7] Huang H, Milione G, Lavery MP, et al. Mode division multiplexing using an orbital angular momentum mode sorter and MIMO-DSP over a graded-index few-mode optical fibre. Sci Rep 2015;5:14931.
[8] Yan Y, Xie G, Lavery MP, et al. High-capacity millimetre-wave communications with orbital angular momentum multiplexing. Nat Commun 2014;5:4876.
[9] Li S, Wang J. Compensation of a distorted N-fold orbital angular momentum multicasting link using adaptive optics. Opt Lett 2016;41:1482–5.
[10] Zhang H, Kang M, Zhang X, et al. Coherent control of optical spin-to-orbital angular momentum conversion in metasurface. Adv Mater 2016;29:1604252.
[11] Cai X, Wang J, Strain MJ, et al. Integrated compact optical vortex beam emitters. Science 2012;338:363–6.
[12] Gregg P, Kristensen P, Ramachandran S. Conservation of orbital angular momentum in air-core optical fibers. Optica 2015;2:267.
[13] Bozinovic N, Ramachandran S. Terabit-scale orbital angular momentum mode division multiplexing in fibers. Science 2013;340:1545–8.
[14] Wang J. Advances in communications using optical vortices. 2016;4:B14–B28.
[15] Jiang Y, Ren G, Lian Y, Zhu B, Jin W, Jian S. Tunable orbital angular momentum generation in optical fibers. Opt Lett 2016;41:3535–8.
[16] Li S, Mo Q, Hu X, Du C, Wang J. Controllable all-fiber orbital angular momentum mode converter. Opt Lett 2015;40:4376–9.
[17] Zhao Y, Liu Y, Zhang L, Zhang C, Wen J, Wang T. Mode converter based on the long-period fiber gratings written in the two-mode fiber. Opt Express 2016;24:1–3.

[18] Zhang W, Huang L, Wei K, et al. High-order optical vortex generation in a few-mode fiber via cascaded acoustically driven vector mode conversion. Opt Lett 2016;41:5082–5.
[19] Richardson DJ, Fini JM, Nelson LE. Space-division multiplexing in optical fibres. Nature Photon 2013;7:354–62.
[20] Van Uden RGH, Correa RA, Lopez EA, et al. Ultra-high-density spatial division multiplexing with a few-mode multicore fibre. Nature Photon 2014;8:865–70.
[21] Kreysing M, Ott D, Schmidberger MJ, et al. Dynamic operation of optical fibres beyond the single-mode regime facilitates the orientation of biological cells. Nat Commun 2011;5:5481.
[22] Li M, Yan S, Yao B, Liang Y, Zhang P. Spinning and orbiting motion of particles in vortex beams with circular or radial polarizations. Opt Express 2016;24:20604–12.
[23] Angelsky OV, Bekshaev AY, Maksimyak PP, et al. Circular motion of particles suspended in a Gaussian beam with circular polarization validates the spin part of the internal energy flow. Opt Express 2012;20:11351–6.
[24] Han Y, Liu YG, Huang W, Wang Z, Guo JQ, Luo MM. Generation of linearly polarized orbital angular momentum modes in a side-hole ring fiber with tunable topology numbers. Opt Express 2016;24:17272–84.
[25] Snyder A, Love J. Optical waveguide theory. New York, USA, Chapman and Hall Ltd Press, 1983.
[26] Wu Z, Wang Z, Liu YG, Han T, Li S, Wei H. Mechanism and characteristics of long period fiber gratings in simplified hollow-core photonic crystal fibers. Opt Express 2011;19:17344–9.
[27] Vial A, Grimault AS, Macías D, Barchiesi D, Lamy DLC, Marc. Improved analytical fit of gold dispersion: Application to the modeling of extinction spectra with a finite-difference time-domain method. Phys Rev B Condensed Matter 2005;71:85416.
[28] Sun Z, Liu Y, Wang Z, et al. Long period grating assistant photonic crystal fiber modal interferometer. Opt Express 2011;19:12913–8.